

Precise control of tibial nerve stimulation for bladder regulation via evoked compound action potential feedback mechanisms

Received: 29 October 2024

Accepted: 16 April 2025

Published online: 02 May 2025



Young-Soo Lim^{1,14}, Ji Hong Kim^{2,14}, Junho Kim^{3,14}, MinhDuc Hoang¹, Wonok Kang^{1,4}, Matthew Koh⁵, Won Hyuk Choi², Steve Park^{6,7}, Unyong Jeong⁸, **Do Hwan Kim**^{2,9,10} ✉ & Sung-Min Park^{1,11,12,13} ✉

Optimizing stimulation protocols for peripheral neuromodulation often depends on patient feedback, which can result in inconsistent clinical outcomes. Here we present a closed-loop control system for peripheral nerve stimulation (PNS) that utilizes evoked compound action potential (ECAP) feedback to regulate stimulation parameters, addressing the limitations of traditional methods. Unlike established closed-loop control techniques in the central nervous system, such as local field potential and spike analysis, a comparable approach for the peripheral nervous system remains underdeveloped. ECAPs can be consistently observed across peripheral nerves, providing a reliable measure of nerve activation. We developed a fully implantable device and neural interface for tibial nerve stimulation (TNS) that incorporates the proposed closed-loop system. This TNS system shows promise as a PNS treatment for alleviating overactive bladder symptoms. In a rat model, the system demonstrated longer micturition intervals and greater effectiveness compared to conventional motor response-based control.

Neuromodulation is a clinical approach that involves the suppression or excitation of target nerves to regulate abnormal neural activity through artificial stimulation, utilizing electrical, magnetic, or ultrasonic energy according to established clinical protocols^{1–3}. To date, various neuromodulation treatments, such as deep brain stimulation (DBS) for Parkinson's disease⁴, transcranial magnetic stimulation (TMS) for psychiatric disorders⁵, and epidural spinal cord stimulation

(SCS) for chronic pain management⁶, have achieved FDA approval and demonstrated statistically significant patient outcomes in modern clinical settings^{7–12}. Traditionally, neuromodulation techniques have been primarily applied to the central nervous system, which presents lower accessibility. However, there is growing interest in the modulation of peripheral nerves, which offer higher accessibility and serve as a critical pathway for neural signals that directly regulate various organs.

¹Department of Convergence IT Engineering (CITE), Pohang University of Science and Technology (POSTECH), Pohang, Republic of Korea. ²Department of Chemical Engineering, Hanyang University, Seoul, Republic of Korea. ³School of Interdisciplinary Bioscience and Bioengineering, Pohang University of Science and Technology (POSTECH), Pohang, Republic of Korea. ⁴Department of Electronic Engineering, Yeungnam University, Gyeongsan, Republic of Korea. ⁵POSTECH Medical Science and Engineering, Pohang University of Science and Technology (POSTECH), Pohang, Republic of Korea. ⁶Department of Materials Science and Engineering, Korea Advanced Institute of Science and Technology (KAIST), Daejeon, Republic of Korea. ⁷KAIST Institute for Health Science and Technology, Daejeon, Republic of Korea. ⁸Department of Materials Science and Engineering, Pohang University of Science and Technology (POSTECH), Pohang, Republic of Korea. ⁹Institute of Nano Science and Technology, Hanyang University, Seoul, Republic of Korea. ¹⁰Clean-Energy Research Institute, Hanyang University, Seoul, Republic of Korea. ¹¹Department of Electrical Engineering, Pohang University of Science and Technology (POSTECH), Pohang, Republic of Korea. ¹²Department of Mechanical Engineering, Pohang University of Science and Technology (POSTECH), Pohang, Republic of Korea. ¹³Institute of Convergence Science, Yonsei University, Seoul, Republic of Korea. ¹⁴These authors contributed equally: Young-Soo Lim, Ji Hong Kim, Junho Kim.

✉ e-mail: dhkim76@hanyang.ac.kr; sungminpark@postech.ac.kr

As a result, research associated with peripheral nerve stimulation (PNS)^{13–15} for chronic conditions such as hypertension^{16,17} and bladder dysfunction^{18–21} is actively advancing. Ongoing investigations aim to expand the clinical applications of PNS, addressing diverse medical needs and improving patient outcomes. These advancements indicate that further refinement of PNS could lead to more precise and effective therapeutic solutions, offering significant potential for personalized treatment.

Currently, PNS protocols are periodically determined by medical professionals who analyze the patient's condition and adjust treatment regimens by modifying factors such as duration, intensity, and stimulation frequency^{22,23}. However, optimal treatment protocols are subject to continuous variation due to the changes in individual physiological conditions, drug interactions, and disease progression stages^{24,25}. Additionally, fluctuations in the electrode-to-nerve interface can significantly impact physiological equilibrium, potentially hindering the acquisition of meaningful outcomes from the applied stimulation²⁶. Despite standardized protocol management across patient groups, achieving consistent outcomes for all individuals remains challenging. This variability is evident in specific studies^{27–29}, which report differences in effectiveness among equivalent groups. Furthermore, there are documented cases^{30–32} of excessive electrical stimulation applied to some individuals within controlled groups, risking tissue and nerve damage. Despite these risks, methods that utilize maximum stimulus intensity at the patient's tolerance level are still practiced. Existing PNS systems often face challenges due to the absence of reliable feedback mechanisms, resulting in suboptimal stimulation parameters and inconsistent therapeutic outcomes. Additionally, these systems struggle to adapt to individual patient variability and continuously fluctuating neurophysiological conditions, reducing their overall efficacy. In this context, the proposed ECAP-based feedback system is poised to offer a more precise and adaptable approach to neuromodulation, enhancing therapeutic outcomes and significantly improving patient satisfaction. The resultant ineffectiveness or adverse effects sometimes outweigh the benefits of neuromodulation. This instability has driven the development of control methods that continuously incorporate relevant physiological feedback^{33–36}, rather than relying on periodic adjustment based on empirical observation or experience.

The technological landscape of neuromodulation is rapidly evolving, driven by the development of bioelectronic systems that enable real-time signal recording and closed-loop control^{1,33,37}. Capturing comprehensive physiological signals enhances the precision of therapeutic interventions by providing quantitative analysis. In particular, neural signal monitoring has led to significant advances in DBS and SCS. The use of local field potential (LFP) and spike analysis for closed-loop control³⁸ has greatly improved the management of conditions mediated by central nervous system disorders. However, while these established interventions have progressed to treat conditions such as epilepsy¹¹ and even hypertension¹⁷, LFP and spike analysis do not effectively translate to the peripheral nervous system, presenting challenges in their adaptation and application. To address the limitations of current PNS, attention must shift toward control systems that leverage measurable and effective features within the peripheral nervous system to maximize the outcomes of neuromodulation.

Here, we propose a closed-loop PNS control system that uses ECAP as quantitative neural feedback to optimize stimulus parameters. This approach offers superior precision and adaptability for direct neural interfacing and has the potential for high scalability across various PNS treatments. Unlike LFP and spike analysis, which typically require complex, high-bandwidth systems and extensive computational resources, ECAP monitoring imposes a significantly lower engineering load while still delivering reliable neural feedback. This makes the proposed approach both efficient and scalable, offering superior precision and adaptability for precise PNS control across various treatments. This versatility stems from relying on nerve signal

feedback—specifically, ECAPs observed across nerve strands—rather than being limited to specific physiological parameters of chronic conditions. The proposed system is designed to be fully implantable, integrating custom-developed devices for measurement and stimulation. It monitors ECAPs from stimulation to assess nerve activation, providing feedback for the control system to adjust stimulus parameters accordingly (Fig. 1a). Additionally, our custom-developed electrodes for neural signal measurement, coated with a hybrid ionic gel (gelatin methacryloyl (GelMA) with choline-malate ionic liquid) on a flexible mesh electrode, enhance neural interfacing compared to conventional metal electrodes. This design improves signal fidelity and electrode stability by offering high capacitance and electrochemical stability. To assess the *in vivo* performance and feasibility of the system, we selected tibial nerve stimulation (TNS) as the application for this closed-loop neuromodulation method. TNS is an emerging treatment for alleviating overactive bladder (OAB) symptoms. In this study, we evaluated the effectiveness of the proposed system by monitoring the controlled bladder activity^{39,40}. We compared the results of TNS using conventional motor response-based methods^{41,42} with those obtained using our ECAP-based control system (Fig. 1b).

Results

System evaluation through TNS application

In clinical settings, TNS treatment is commonly used to alleviate symptoms of urinary disorders, such as urinary incontinence and OAB⁴³. TNS aims to reduce detrusor muscle overactivity and relieve symptoms of urgency and frequency in the bladder. Although the precise mechanism of TNS remains uncertain, it is believed that this effect may stem from the modulation of afferent signals triggered by bladder distention, leading to the maintenance of bladder continence^{43–45}. By monitoring bladder activity through intra-bladder pressure (IBP) measurement, we conducted a quantitative analysis of the increased micturition interval achieved by the applied stimulation. Measurement data collected during stimulation was excluded due to susceptibility to electrical artifacts, which could interfere with the interpretation of genuine physiological responses. To ensure accuracy, data from the post-stimulation window were analyzed, allowing for a clearer and more reliable assessment of micturition patterns.

The proposed bioelectronic system was specifically designed for TNS, with an implantable device and electrode configuration tailored to meet the requirements of TNS therapy. The system delivers electrical stimulation to the tibial nerve, while response signals are measured from the sciatic nerve to assess neural activity. Using ECAP analysis, detailed in the Methods section, the system adjusts the stimulus intensity to ensure precise control and effective neuromodulation. While traditional TNS relies on toe tremor as a criterion for determining stimulus intensity, the proposed system uses ECAP as a feedback feature to analyze nerve activation increment as the selection criterion. Traditional TNS systems determine stimulus intensity based on toe tremor, whereas the proposed system leverages ECAP as a feedback feature to assess nerve activation increments as the selection criterion. This approach reduces the need for repeated adjustments to reach an appropriate threshold, addressing the limitations of traditional methods, which can be time-consuming and less efficient in optimizing stimulus intensity. To evaluate the performance of the proposed feedback-based stimulation optimization system, motor response (toe tremor) was monitored via EMG for comparison with the conventional method.

Threshold evaluation for stimulation intensity control

The experiment protocol, shown in Fig. 2a, outlines the threshold testing phase conducted to evaluate the motion threshold and the ECAP threshold for each subject. During this test, stimulus intensity was incrementally increased (in 5 μ A steps, from 20 to 255 μ A, within a safe range for direct nerve stimulation⁴⁶) while nerve signal and EMG responses were continuously measured. Our experiment employed a

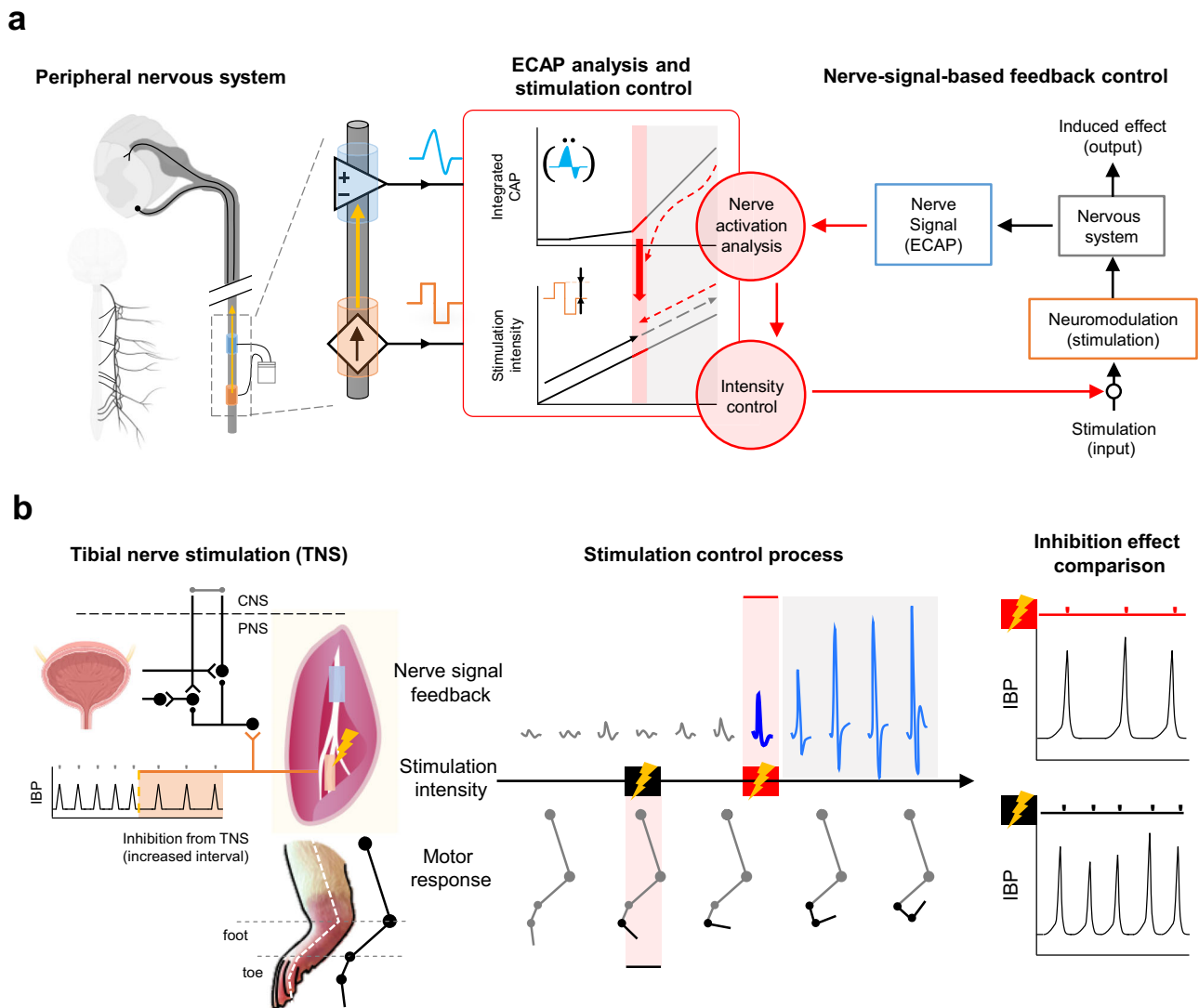


Fig. 1 | Overview of ECAP-based control system. **a** Diagram of the nerve signal analysis feedback-based system. The system stimulates the nerve and measures the nerve signal. ECAP signals are captured for analysis, and stimulation is controlled based on ECAP feedback. **b** Representative diagram illustrating the system

evaluation in a TNS application. Comparison of micturition interval changes by stimulation control method: conventional method (motor response) vs. proposed method (ECAP-based feedback). (* IBP: intra-bladder pressure) Created in BioRender. Rachim, V. (2025) <https://BioRender.com/3p6au1k>.

nerve cuff electrode and low-intensity stimulation, minimizing unintended current spread. Given the anatomical distance of the tibial nerve from major visceral organs and the absence of motor responses even at proximal muscles, influence to unintended targets are unlikely.

Figure 2b presents the threshold analysis results from representative data obtained during the test. The top plots show the EMG and nerve signal response relative to the applied stimulus intensity. The motion threshold was defined as the stimulus intensity at which EMG activation occurred, while the ECAP threshold was determined by a significant increase in the ECAP amplitude, as analyzed through the rate of change in the integrated ECAP. The threshold test ensured the accurate measurement and confirmation of both thresholds, with the motion threshold averaging $94 \pm 2.2 \mu\text{A}$ and the ECAP threshold averaging $117 \pm 4.5 \mu\text{A}$. Figure 3a shows the motion threshold and ECAP thresholds measured from eight rats, consistently indicating that the motion threshold was lower than the ECAP threshold. Comprehensive analysis data can be found in supplementary information (Supplementary Fig. 1 and Supplementary Table 1).

The tibial nerve, which branches from the sciatic nerve, consists of both motor and sensory nerves, encompassing various types of nerve fibers^{47,48}. These fibers have distinct physical and electrophysiological

characteristics. As fiber diameter decreases and myelination reduces, progressively higher stimulus intensities are required to activate and propagate action potentials, in the following order: $\text{A}\alpha$ -, $\text{A}\beta$ -, $\text{A}\delta$ -, and C-fibers⁴⁹. The afferent innervation of the urinary bladder primarily involves $\text{A}\delta$ and C fibers^{50,51}, while motor responses arise from $\text{A}\alpha$ fibers⁵². The higher ECAP threshold compared to the motion threshold suggests that additional nerve fibers were activated as the ECAP threshold was reached. This approach allows for more precise intensity adjustments by using ECAP as a specific physiological marker, offering quantitative control superior to traditional methods.

TNS effectiveness comparison for system evaluation

For treating OAB, reducing urinary frequency is one of the important factors. In the main experiment, the effectiveness of micturition interval increase was compared between groups stimulated at the motion threshold and ECAP threshold intensities. Figure 2c shows a representative micturition pattern measured during this phase. Motion threshold stimulation was conducted first, followed by ECAP threshold stimulation, with a resting period of at least 1 h between trials to minimize residual effects. IBP was monitored throughout the experiment to assess micturition activity and compare results from

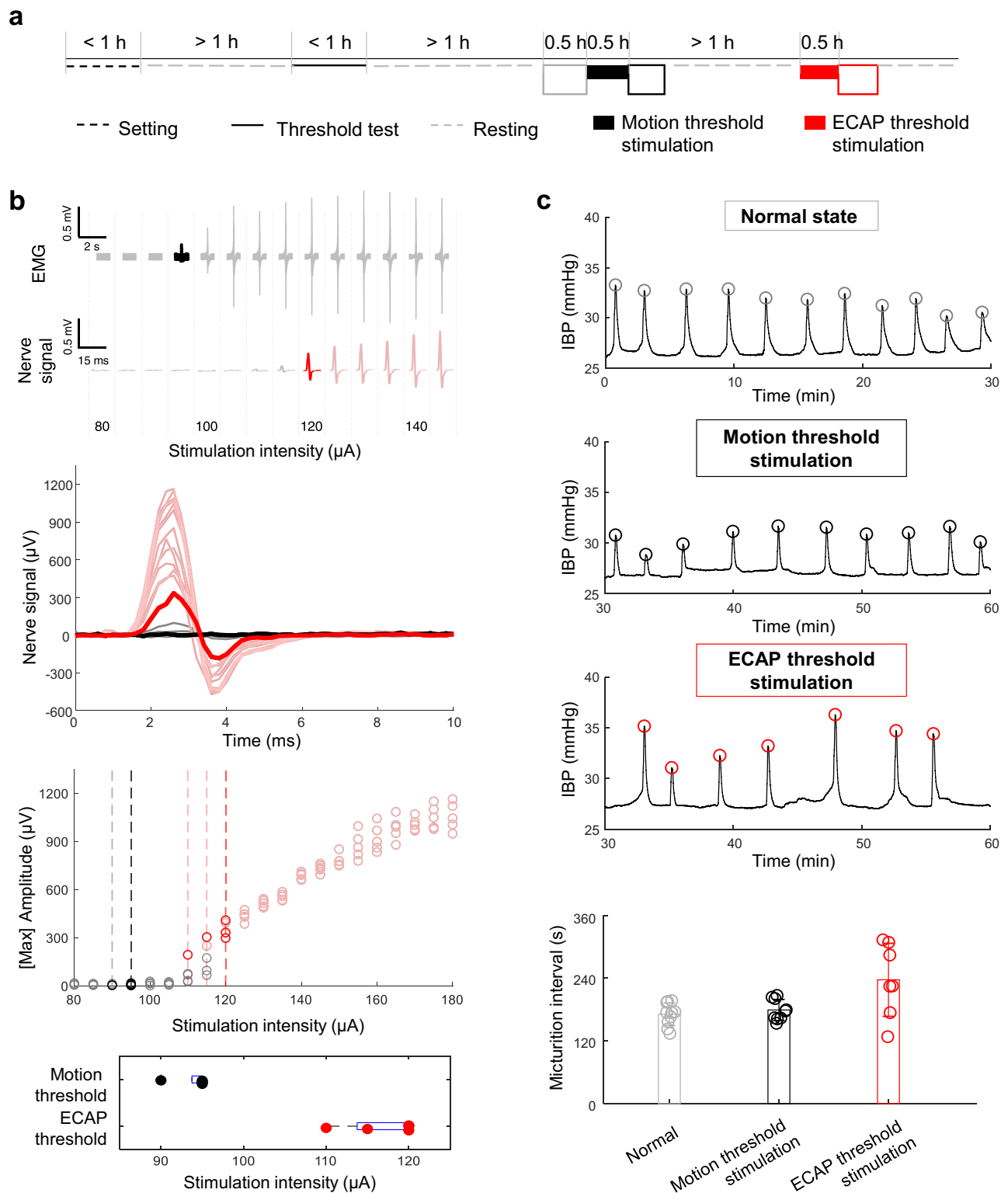


Fig. 2 | Application of the proposed system for TNS compared to the conventional motor-response method. **a** Experimental protocol for the acute condition evaluation. A threshold test is performed in the preliminary phase, followed by the main experiment where stimulation trials are conducted using the evaluated threshold. **b** Process of the threshold test for evaluating motion threshold from EMG and

ECAP threshold from nerve signal measurements (technical $n = 5$). Representative data of subject #1. **c** Micturition patterns from intra-bladder pressure (IBP) monitoring, showing normal state, motion threshold stimulation, and ECAP threshold stimulation. Micturition intervals were analyzed for TNS effectiveness comparison. Data are presented as mean values \pm SD. Representative data of subject #1.

stimulation trials with the normal state. The bottom subplot illustrates the result of the micturition interval analysis. Motion threshold stimulation resulted in a marginal increase in micturition interval, whereas ECAP threshold stimulation led to a 38% increase compared to

the normal state (normal: 171.1 ± 21.6 s, motion threshold: 179.2 ± 20.2 s, and ECAP threshold: 237.0 ± 69.9 s).

Figure 3b presents the analyzed micturition interval results from the normal state, motion threshold stimulation, and ECAP threshold

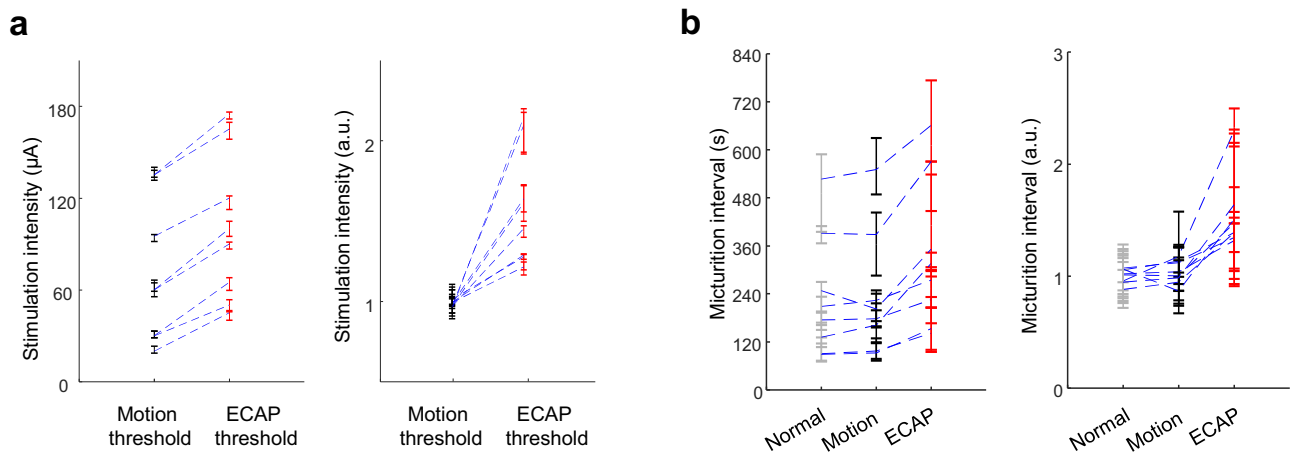


Fig. 3 | Analysis of threshold test and micturition interval. a Motion and ECAP thresholds for each rat ($n = 8$) measured during the threshold test. Data are presented as mean values \pm SD and plotted with median values. Left: actual values,

Right: normalized analysis. **b** Results of micturition interval analysis for each rats ($n = 8$). Data are presented as mean values \pm SD and plotted with mean values. Left: actual real values, Right: normalized analysis.

stimulation across eight rats. While motion threshold stimulation resulted in less than a 10% increase in the micturition interval, ECAP threshold stimulation achieved a significant increase. In addition to its profound effectiveness, a pattern of micturition suppression was exclusively observed with ECAP threshold stimulations (Supplementary Fig. 1 and Supplementary Table. 1). Micturition suppression, characterized by increased pressure and retention, was observed in rats 5–8. However, these rats regained normal micturition reflexes within 30 min post-stimulation, indicating that the proposed stimulation modality induces a transient, acute, and fully reversible response. This suppression aligns with the previously reported prolonged bladder-inhibitory effect^{53–55}, which was also fully reversible and did not cause long-lasting impairments in bladder function.

Previous studies^{47–52} have explained variations in electrophysiological characteristics and functional roles based on the specific types of nerve fibers. Nerve responses after the stimulus pulse were consistently observed within the signal window, gradually increasing as the stimulus intensity rose. The significant increase in ECAP amplitude observed at the ECAP threshold is likely attributed to the activation of additional nerve fibers during action potential propagation. At stimulus intensities reaching the ECAP threshold, more nerve fibers are activated, leading to a cumulative rise in ECAP amplitude as their activation thresholds are progressively met. However, the variation among activated nerve fiber types suggests that stimulus intensity at the motion threshold may be insufficient to achieve the desired neuromodulation effect, as it may not engage enough necessary fibers to produce the intended therapeutic outcome.

These findings highlight the limitations of conventional methods. Motor responses often fail to correlate with optimal therapeutic outcomes, resulting in inadequate neuromodulation effects. When the initial stimulus intensity is insufficient, it is manually increased to achieve the desired therapeutic effect. However, motor responses lack precision in this adjustment process. In contrast, the proposed approach enables more precise adjustments by incorporating quantitative feedback from ECAP analysis, resulting in more targeted neuromodulation. Our experimental results demonstrated that the proposed system achieves better alignment with the desired outcomes than the conventional method.

Device validation for operation in implant conditions

The custom implantable device's circuitry comprises a microcontroller unit and an electrophysiology interface, enabling the integrated operation of nerve stimulation and signal measurement. It also features wireless communication and wireless power transfer (WPT) for

use under implanted conditions. The device was assembled in a custom-designed packaging case that includes a WPT transmission coil and a Li-Po battery (Fig. 4a). This case is designed to provide both hermetic sealing and allow radio frequency signal penetration. Wireless control, data transfer, and WPT were successfully tested in vivo before the implantation experiment. Figure 4b shows the results of a temperature test conducted during maximum amplitude stimulation and WPT charging. The temperature increased by 0.7 °C after 30 min and by 1.2 °C after 1 h. Under idle conditions, the temperature increased by 0.6 °C after 6 h. During the implanted operation, the temperature rose by 1.1 °C following the protocol, remaining below the 2 °C safety limit for implantable medical devices⁵⁶.

Power consumption was primarily attributed to the electrophysiology interface's operation. Power consumption during full operation (stimulus pulse signal generation at maximum amplitude) was measured at 86.8 mW, while idle condition consumption was 48.5 mW (Fig. 4c). The system remained fully operational for 5 h and could maintain idle mode for 2 days without recharging. During WPT charging, the system was operational for over 12 h, since the TNS protocol required stimulation for only 30 min, charging during operation was unnecessary.

Nerve signal measurement cuff electrode

Flexible electrodes for neural signal recording are designed to closely match the mechanical properties of neural tissue, reducing mechanical mismatches and thereby minimizing inflammation and potential long-term damage. Their flexibility enhances tissue integration and increases the contact area between electrode and tissue, which improves charge transfer and enhances sensitivity for neural signal detection. Another critical feature of these electrodes is their ability to maintain electrical stability over extended use, preventing performance degradation. This combination of mechanical compliance and long-term electrical stability makes flexible electrodes ideal for reliable, long-term neural interfacing, optimizing signal detection while reducing tissue damage. To meet the necessary characteristics for such recording electrodes, an equivalent circuit model of the tissue-electrode interface in bioelectronics is shown in Fig. 5a. For recording purposes, the most critical factor is achieving a high recording voltage (V_{rec}). The voltage signal (V_e), generated by ionic currents from action potentials (IAP) in the extracellular medium, passes through the tissue-electrode interface, which comprises contact resistance (R_c) and electrical double-layer (EDL) capacitance. Therefore, lower R_c and higher EDL capacitance at the electrode interface are essential to ensure effective recording electrodes.

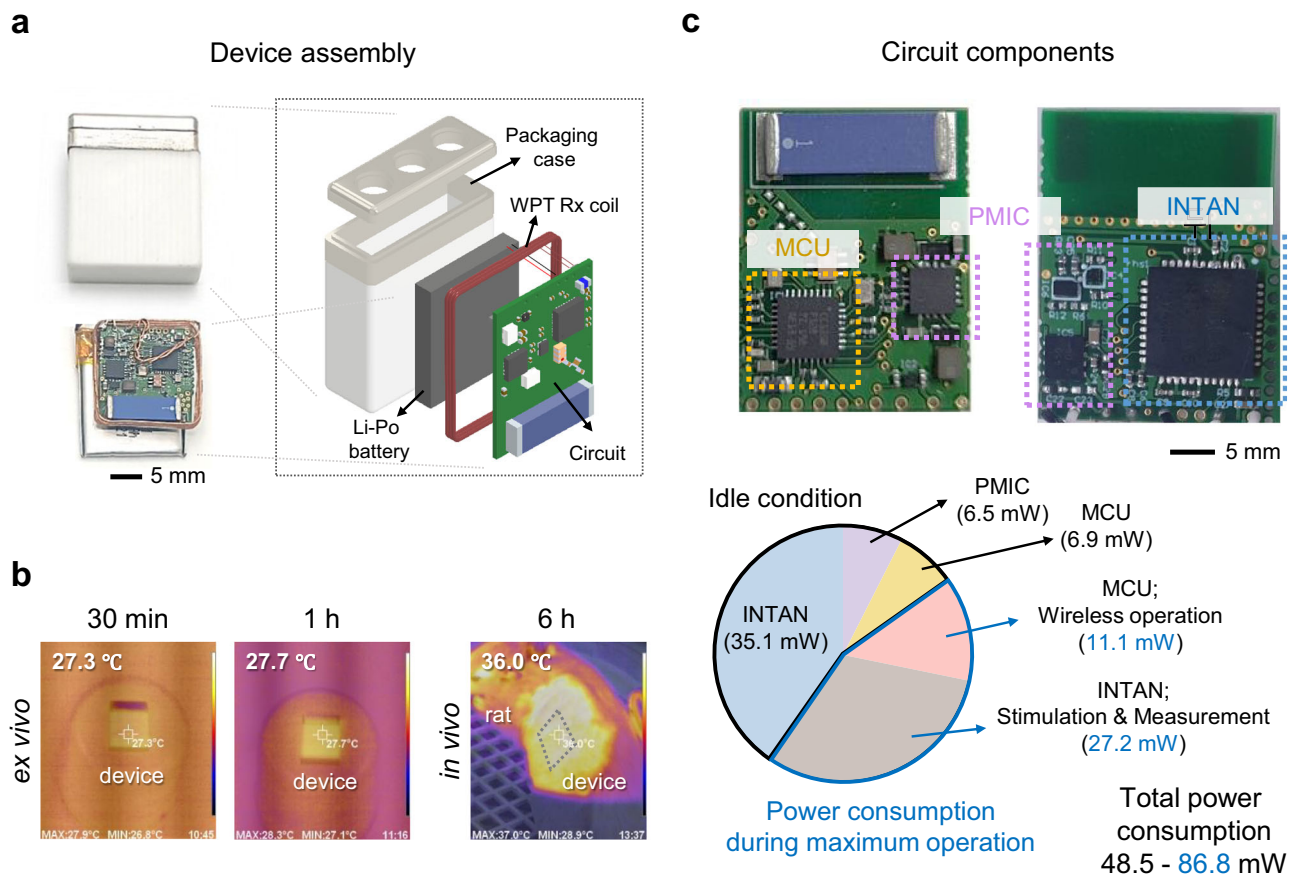


Fig. 4 | Device evaluation of temperature and power consumption for implant operation. **a** Packaging case, battery, WPT Rx coil, and circuit components for device assembly. Black bar: 5 mm. **b** Temperature test results after device's maximum operation of 30 min and 1 h, and during implanted operation for 6 h. **c** Power

consumption of the device; idle condition and maximum operation. Stimulation parameters during maximum operation: biphasic, 255 μ A amplitude, 100 μ s pulse width, and 20 Hz frequency. Black bar: 5 mm.

To achieve these properties, we fabricated an ion-gel-coated, stretchable Au electrode on an elastic nanofiber mesh. The ion gel, made from GelMA biopolymer combined with choline malate ionic liquid, provides high EDL capacitance. This ion gel was stably coated onto the stretchable Au electrode via photo-crosslinking (Fig. 5b and Supplementary Fig. 4)⁵⁷. Figure 5c shows the thickness variation of the Au mesh electrode before coating (Au MESH) and after applying the GelMA ion gel (GelMA MESH), as measured by AFM, with thickness increasing from ~2 to 4 μ m. The GelMA ion gel, with a high ionic content (80 wt%) on the mesh, exhibited a modulus of 87.3 kPa, similar to human nerve tissue (Supplementary Fig. 5)⁵⁸. Additionally, the integration of the ion gel coating showed a stress relaxation effect due to the viscoporoelastic properties of the ion gel (Fig. 5d)^{59,60}. The stress on the Au MESH initially decreases and then stabilizes over time. In contrast, the GelMA MESH, and the GelMA MESH after soaking in phosphate-buffered saline (PBS) to simulate physiological conditions, showed a progressive reduction in stress magnitude over time, indicating that the force applied by the electrode on the nerve gradually diminishes.

Next, the electrical stability of the GelMA MESH was evaluated under varying strain rates. For the Au MESH, the resistance remained relatively stable at lower strain levels but it increased sharply when strain exceeded 50% (Fig. 5e and Supplementary Fig. 6). This behavior is attributed to the cracks forming in the electrode as the spacing between sputtered Au layers on the mesh expanded under tensile stress. In contrast, the GelMA MESH exhibited superior mechanical resilience, as the tensile force was effectively distributed through the ion gel coating. Even at 100% strain, the initial resistance remained

largely unaffected, indicating excellent strain tolerance of the GelMA MESH. Additionally, at a maximum strain of 20%—the highest stress typically endured by human nerves^{61,62}—repeated cyclic testing showed that the Au MESH could not maintain its initial resistance beyond 100 cycles, with a sharp increase in resistance observed. In contrast, the GelMA MESH exhibited outstanding stability, retaining its initial resistance even after 1000 cycles (Supplementary Fig. 7). This highlights the superior mechanical durability of the GelMA MESH under repetitive strain conditions, demonstrating its potential for long-term cyclic loading.

The electrochemical stability of the GelMA MESH was assessed through multiple charge-discharge cycles using cyclic voltammetry (CV). To evaluate electrochemical performance, the GelMA MESH was immersed in PBS and used as a working electrode during CV measurements (Fig. 5f). For the Au MESH, capacitance formation was primarily attributed to ion accumulation at the Au-PBS interface, resulting in surface-limited capacitance. In contrast, the GelMA MESH benefited from the high volumetric capacitance of the GelMA ion gel, leading to a significantly higher current density (Fig. 5g). Moreover, during repeated charging and discharging cycles, the Au MESH exhibited substantial variations in initial current values and charge storage capacity due to redox reactions after 1000 cycles. By comparison, the GelMA MESH maintained stable current density and charge storage capacity, even after 1000 cycles, demonstrating superior electrochemical stability (Fig. 5h). These findings further support the use of GelMA-coated flexible electrodes in long-term neural interfacing applications, where both mechanical compliance and electrical reliability are essential for optimal performance.

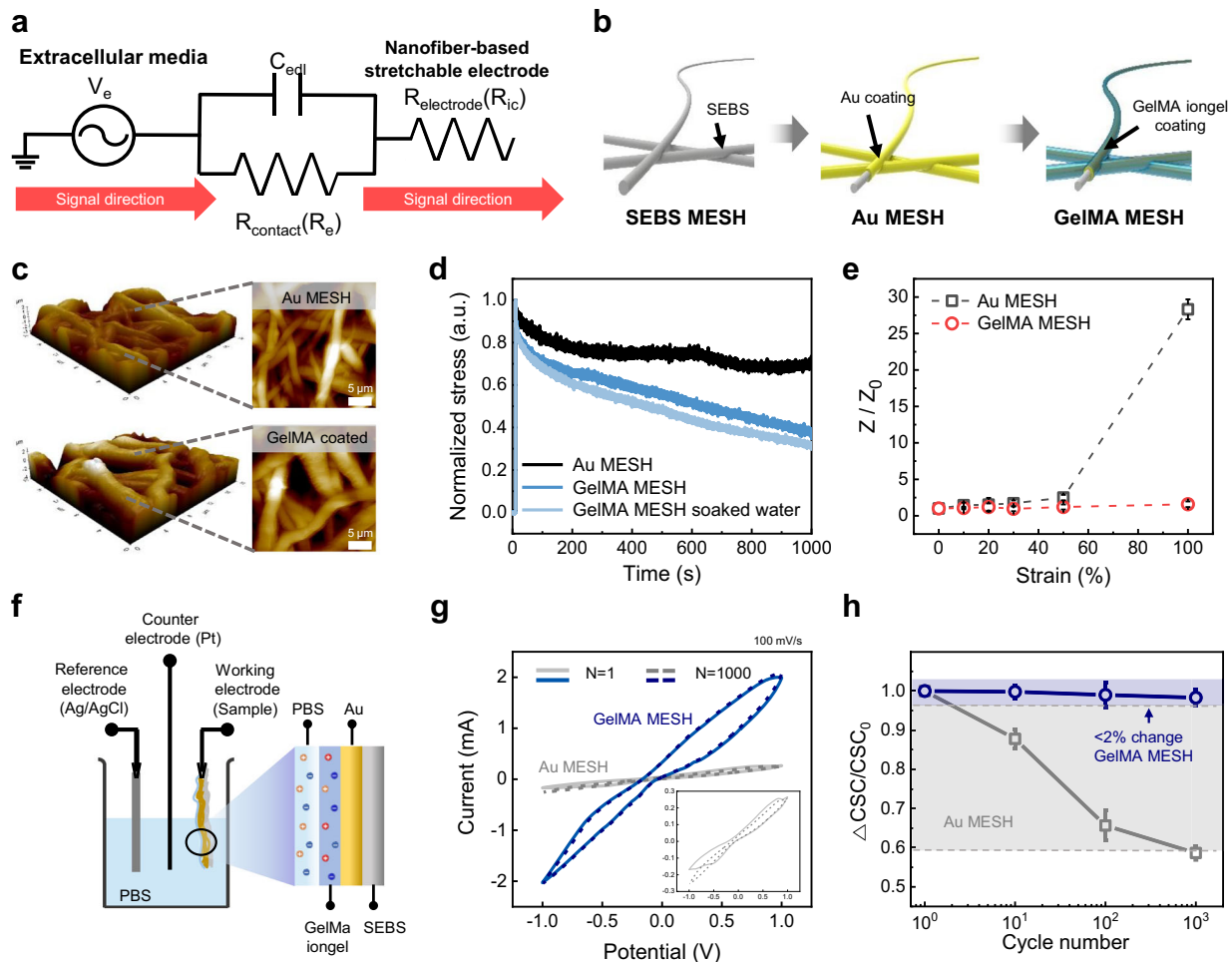


Fig. 5 | Mechanical and electrochemical stability of the GelMA MESH recording electrode. **a** Equivalent circuit design of the human tissue and electrode interface for the recording electrode. **b** Schematic of the stretchable electrode fabrication sequence. The electrode was manufactured by coating gold onto a SEBS mesh and then coating it with ion gel. **c** 3D and 2D atomic force microscopy (AFM) images of Au MESH and GelMA MESH stretchable electrodes. **d** Time-dependent stress–relaxation behavior of the electrodes before and after soaking in PBS for 0–1000 s. **e** Impedance changes in the stretchable electrode under strain.

f Schematic illustration of the three-electrode cyclic voltammetry (CV) setup used to analyze the stability of the stretchable electrode. Au MESH and GelMA MESH were soaked in PBS solution as the working electrode. Data are presented as mean values \pm SD. **g** CV curve comparison between Au MESH and GelMA MESH during multiple cycles of charging/discharging. **h** Charge storage capacity (CSC) changes in Au MESH and GelMA MESH during various cycles. Data are presented as mean values \pm SD.

System evaluation in an implanted freely moving rat

The custom-developed device and electrode were carefully designed to meet the requirements for a fully implantable system. This process involved optimizing both their functional capabilities and physical characteristics to ensure stable performance in the *in vivo* environment while achieving effective neuromodulation. The validation process included rigorous testing and refinement to ensure that both the device and electrode could withstand the implanted condition, ensuring successful implementation for the selected TNS application.

The system was assembled and implanted into a freely moving rat according to the procedure outlined in the Methods section. After a recovery period of 3-day post-implantation, the rat underwent the experiment protocol outlined in Fig. 6b for evaluation in a freely moving state. Nerve signals measured under the implantation condition successfully distinguished the ECAP threshold (Fig. 6c). Figure 6d shows the result of the threshold test and micturition interval comparison in the freely moving rat. The results revealed a lower motion threshold (motion threshold: $48 \pm 2.7 \mu\text{A}$, ECAP threshold: $71 \pm 2.2 \mu\text{A}$) and greater effectiveness during ECAP threshold stimulation (ECAP micturition interval change: $140.9 \pm 13.9 \text{ s} \rightarrow 235.0 \pm 64.7 \text{ s}$). These results, which closely match those observed in previous acute tests,

demonstrate the robustness and adaptability of the system under dynamic conditions. The successful distinction of ECAP thresholds and the consistent effectiveness in the freely moving rat strongly indicate the system's reliability with more natural, real-world settings. The effective performance of the fully implanted system suggests that it can be adapted for other PNS applications, highlighting the scalability of our approach.

Tissue response evaluations further confirmed the electrode's stability and biocompatibility. Throughout the two-month implantation period, no behavioral abnormalities were observed. Post-excision histological analyses also revealed no signs of inflammation, adhesions, or nerve deformation at the implantation site (Supplementary Fig. 9). These findings underscore the system's reliability for long-term applications and support its potential for clinical translation.

Discussion

Neuromodulation offers a promising alternative for managing a range of neurological disorders, though its clinical success hinges on the precise optimization of stimulation protocols. This study presents an ECAP-based feedback control system as a foundation for closed-loop PNS control, addressing limitations in traditional PNS

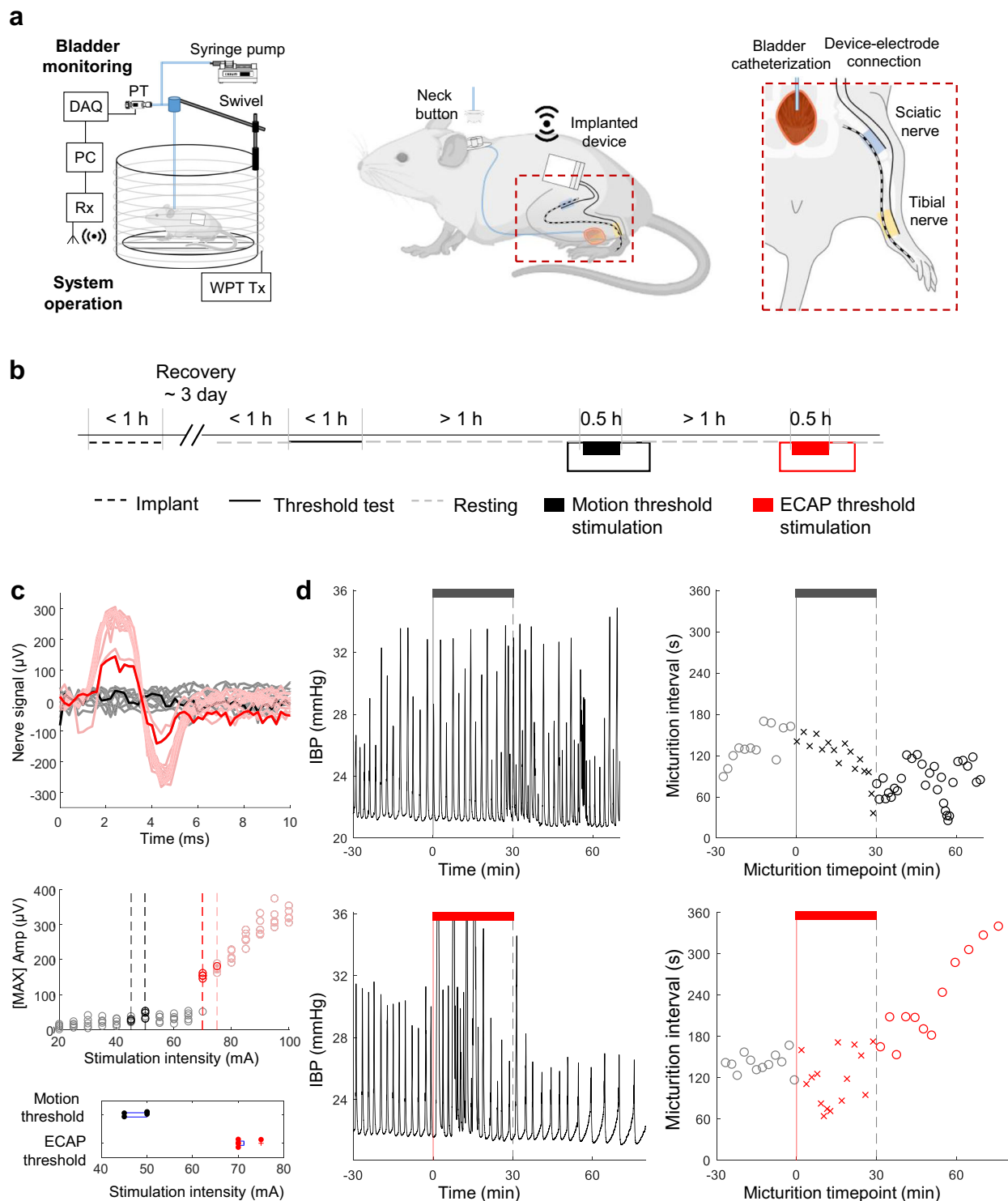


Fig. 6 | System evaluation with fully implanted freely moving rat. a Overview of the system evaluation in implanted condition. **b** Experiment protocol for the freely moving rat. The rat underwent the same procedure as the acute experiment after a 3-day recovery period. **c** Nerve signal measurement and ECAP analysis in implanted conditions. Motion and ECAP thresholds were evaluated. **d** Comparison of

micturition patterns between motion threshold stimulation and ECAP threshold stimulation. The plot shows micturition time points and intervals for TNS effectiveness analysis. (* IBP: intra-bladder pressure) Created in BioRender. Rachim, V. (2025) <https://BioRender.com/3p6aulk>.

methods, which rely on patient responses or sensory and motor feedback. We developed a fully implantable device featuring hermetic sealing, wireless charging/communication, and a soft electrode for long-term, stable neural interfacing. This system was evaluated in the context of TNS, an emerging neuromodulation approach for managing overactive bladder syndrome, and its efficacy

was thoroughly tested in a freely moving rat study. The results showed that stimulation based on the ECAP threshold extended micturition intervals more effectively than motion threshold-based stimulation. The higher stimulation intensity at the ECAP threshold, compared to the motion threshold, likely contributes to a more pronounced output response. This enhanced efficacy is likely due to

broader nerve fiber activation at the ECAP threshold, including fibers that contribute more effectively to neuromodulation.

The system also holds potential for personalized control across various PNS applications by using neural signal feedback for precise modulation, independent of physiological symptoms. The ECAP-based tibial nerve modulation technique proposed in this study represents a distinct approach from conventional methods, requiring further investigation before clinical application. While this study primarily validated the proposed TNS in a rat model, translating it into clinical use presents several challenges. The selection of male rats introduced anatomical and technical constraints in assessing detailed responses, such as urodynamics and urethral resistance. These include demonstrating therapeutic efficacy in humans, overcoming the complexities of implanting cuff electrodes for invasive nerve access, and mitigating long-term degradation of fully implanted systems. Ensuring long-term biocompatibility, optimizing minimally invasive implantation techniques, and addressing anatomical variability in human peripheral nerves remain critical hurdles in advancing this technology toward human clinical trials. To support clinical translation, biocompatible materials with excellent mechanical and electrical stability, including SEBS, Au, and GelMA ion gel, were incorporated. These materials, rigorously validated for *in vivo* safety and biocompatibility, minimize tissue damage during implantation while ensuring sustained, reliable performance over extended periods. However, enhancing the system's versatility and scalability necessitates further exploration of advanced minimally invasive approaches, such as laparoscopic-assisted procedures. Addressing challenges such as optimizing implantation techniques for safety and accommodating anatomical variations in human peripheral nerves will be essential. Also, for actual clinical translation, long-term safety and stability must be directly tested in human applications. Additionally, during clinical use, lasting follow-up monitoring of tissue responses to the implanted electrode will be essential for each patient. Future research should aim to develop a real-time closed-loop system and test it in diverse PNS scenarios. Such advancements could eliminate preliminary calibration phases, improve system responsiveness, and reduce the time needed to achieve effective neuromodulation in clinical settings. The ECAP-based feedback system can be adapted for various bioelectronic therapies, including chronic pain management with peripheral nerve stimulation and hypertension and epilepsy treatment with vagus nerve stimulation. By enabling more precise neuromodulation through the targeted regulation of specific neural responses, this approach enhances therapeutic efficacy across multiple clinical applications. In summary, this study demonstrates that the proposed ECAP-based feedback control system enables more precise TNS, improves outcomes, and lays the groundwork for advanced PNS control techniques to manage a variety of chronic conditions associated with neurological disorders.

Methods

Device firmware

The device is operated by a CC1350 microcontroller unit (Texas Instruments Inc.), which controls the RHS2116 electrophysiology interface (Intan Technologies). RHS2116 is capable of simultaneous recording and stimulation with isolation circuitry. The firmware is written in Code Composer Studio (v12, Texas Instruments Inc) and is controlled via a LabView GUI (National Instruments Corp.). A development kit (Texas Instruments Inc.) was used to establish the wireless connection for the PC-controlled operation of the device. From the host PC, the GUI facilitated control of the device functions, allowed for adjustments to the stimulus parameters, displayed measurement results, and enabled data transfer for further analysis.

ECAP threshold analysis and stimulation control

Measurement results transferred from the device were analyzed to capture the ECAP response for ECAP threshold evaluation. The ECAP

signal was integrated to quantify nerve activation. ECAP threshold was determined as the point where the second derivative of the integrated ECAP signal exceeded twice the value of the previous results, indicating a significant increase. The ECAP threshold value was selected as the stimulus intensity, and nerve signals were continuously monitored to ensure that the ECAP signal level was maintained throughout the stimulation.

Circuit development

The device was designed to withstand implantation conditions and was powered by a 3.7 V Li-Po battery, with an option for WPT charging. A 3.3 V low-dropout regulator (ADP151, Analog Devices Inc.) was integrated to ensure the proper operation of the main chips. Additionally, a ± 5 V buck-boost converter (LT3582, Analog Devices Inc.) was used to generate the biphasic signal required for stimulation. For wireless communication, a 433 MHz antenna (ANT1204, Pulse Electronics) was incorporated. Function diagram of the circuitry design is shown in Supplementary Fig. 2. The PCB size was 15 mm \times 18 mm.

Wireless power transfer design

The wireless power system was designed with a dedicated WPT Rx coil for the device. A WPT Tx coil was integrated into the cylindrical cage, with both coils tuned to a frequency of 6.78 MHz. The device incorporated a linear voltage regulator (XCM414, Torex Semiconductor Ltd.) to enable WPT charging of the battery. The WPT Rx coil was designed to wrap around the edges of the PCB, optimizing space utilization with dimensions of 17 mm \times 20 mm. WPT Tx coil was connected to a wireless power amplifier (EPC9512, Efficient Power Conversion Corp.) and a DC power supply (PWS4305, Tektronix Inc.) for WPT charging.

Packaging case

The packaging comprised biocompatible materials—ceramic and Kovar—which were brazed together for seamless welding for implanted conditions. The design prioritizes non-metallic (ceramic) parts, covering over 80% of the case's surface area, to enhance wireless connection efficiency. The case lid was also made from Kovar, with a feedthrough (SA271082 Rev3, Morgan Advanced Materials) incorporated for electrode connections. The case was laser welded after the assembly for hermetic sealing. The dimensions of the packaging case are 20 mm \times 25 mm \times 8 mm, including the lid.

Electrode fabrication

GelMA MESH was prepared in three main steps: (i) SEBS MESH fabrication, (ii) Au deposition, (iii) GelMA ion gel photo crosslinking. In the first step, a 10 wt% solution of SEBS-g-MA was prepared using a solvent blend of cyclohexane, THF, and DMF in a weight ratio of 7:1:2 (Sigma-Aldrich). The solution was electrospun onto an aluminum substrate at a controlled feed rate of 1 mL/h under an applied voltage of 18.0 kV, using an electrospinning apparatus. The setup included a 22 G nozzle, with a nozzle-to-collector distance of 15 cm. After forming a 50 μ m thick fiber mat, it was peeled from the substrate. To initiate imidization, the fiber mat was submerged in a 10 wt% PEI (Sigma-Aldrich) solution in ethanol and maintained at 70 °C for 10 h. This prolonged immersion allowed complete infiltration of PEI into the nanofibers. After retrieval, the mat underwent ultrasonication for 30 min to eliminate excess PEI, followed by drying at ambient temperature. Subsequently, the imidized mat was treated with a 10 wt% solution of (3-aminopropyl)triethoxysilane (APTES, Sigma-Aldrich) in ethanol for 2 h at 70 °C. Post-treatment, the mat was rinsed with DI water and ultrasonicated again for 30 min to remove any unreacted components. In the second step, Au was deposited onto the amine-modified nanofiber mat through a mask. The deposition was achieved via sputtering at 20 mA for 500 seconds using a DC magnetron sputtering system⁵⁷. In the third step, GelMA polymer solution was prepared with 10% (w/w) GelMA (mol wt 95 kDa, degree of substitution 60%, Sigma-Aldrich,

Saint Louis, MO, USA) in DI water. The prepared GelMA polymer solution was supplemented with 1 wt/vol% of the photoinitiator (Irgacure 2959, Sigma-Aldrich), relative to the GelMA solution, and 80% (w/w) of choline malate ionic liquid, relative to the GelMA polymer. The combined solution was heated at 60 °C and stirred at 100 rpm for 4 h, after which the pre-fabricated Au MESH electrode was dipped into the solution for 1 min. The dipped Au MESH electrode is exposed to UV light (365 nm, 25 mW/cm²) for 1 min to fabricate the GelMA MESH. The fabricated GelMA MESH electrode, measuring 0.5 × 1 cm², was integrated with gold nanowires (AuNWs) at both terminal ends, serving as the working electrode on one side and the ground electrode on the other. To reduce noise interference, the AuNWs were encapsulated in a PDMS coating during fabrication. The resulting GelMA MESH electrode was designed to wrap around the nerve, functioning similarly to a cuff electrode for targeted neural stimulation.

Rat preparation

All procedures were approved by the Pohang University of Science and Technology Institutional Animal Care and Use Committee (POSTECH IACUC, POSTECH-2024-0026). Sprague–Dawley rats (270–300 g weight, 8 weeks old, male, animal vendor; Orient Bio Inc.) were used in the study. The rat underwent short-term anesthesia with isoflurane (Piramal Critical Care, Inc.) for the surgical procedure (2% isoflurane, 0.5–0.6 L/min flow rate, 30–40 min). Following surgery, anesthesia was switched to urethane (Sigma-Aldrich) via intraperitoneal injection (20% urethane saline solution, 1.0–1.2 g/kg) to maintain autonomic system function for the micturition reflex.

The syringe pump continuously infused saline intravesically at a constant flow rate of 0.1 mL/min throughout the experiment. This method was chosen to simulate natural bladder filling and ensure stable IBP measurements. During the experimental setup, normal micturition was identified by rhythmic bladder contractions, characterized by periodic IBP peaks. Conversely, cases exhibiting irregular or continuous leakage from the urethra were classified as failed micturition and excluded from analysis.

The sciatic nerve was accessed via the outer thigh, where a custom-developed cuff electrode was placed for measurement. Similarly, the tibial nerve was accessed via the ankle region, and a nerve cuff electrode (NC-1-2-250SS-1-2-Sut-20SS, Microprobes for Life Science) was applied for stimulation. The tibial nerve, a branch of the sciatic nerve, consists of motor and sensory fibers, including A α , A β , A δ , and C fibers. Among these, A δ and C fibers play a primary role in bladder innervation, while A α fibers are responsible for motor responses.

The rat bladder was exposed and catheterized, with the catheter connected to a pressure transducer (BP-100, iWorx System Inc.) and a syringe pump (Pump 11 Elite I/W Dual; v3.0.6, Harvard Apparatus) for controlled monitoring of IBP. A DAQ module (IX-RA-834, iWorx System Inc.) and LabScribe (v3, iWorx System Inc.) were used for physiological measurement.

For the freely moving rat, additional surgical procedures were required. The catheter was extended and connected to a neck button (Instech Laboratories, Inc.) to minimize movement interference and secure the catheter connection from inside the body to the external environment. The device was implanted in the subcutaneous lumbar region, maintaining connection with the electrodes. Incisions made during the surgical process were sutured and sanitized before the rat was allowed to recover from isoflurane anesthesia.

Reporting summary

Further information on research design is available in the Nature Portfolio Reporting Summary linked to this article.

Data availability

All data supporting the findings of this study are available within the article and its supplementary files. Any additional requests for

information can be directed to, and will be fulfilled by, the corresponding authors. Source data are provided with this paper.

References

- Birmingham, K. et al. Bioelectronic medicines: a research roadmap. *Nat. Rev. Drug Discov.* **13**, 399–400 (2014).
- Berggren, M., Glowacki, E. D., Simon, D. T., Stavriniou, E. & Tybrandt, K. In Vivo Organic Bioelectronics for Neuromodulation. *Chem. Rev.* **122**, 4826–4846 (2022).
- Luan, S., Williams, I., Nikolic, K. & Constandinou, T. G. Neuromodulation: present and emerging methods. *Front. Neuroeng.* **7**, (2014).
- Schwalb, J. M. & Hamani, C. The history and future of deep brain stimulation. *Neurotherapeutics* **5**, 3–13 (2008).
- Connolly, K. R., Helmer, A., Cristancho, M. A., Cristancho, P. & O'Reardon, J. P. Effectiveness of transcranial magnetic stimulation in clinical practice post-FDA approval in the United States: results observed with the first 100 consecutive cases of depression at an academic medical center. *J. Clin. Psychiatry* **73**, e567–e573 (2012).
- Yeung, A. M. et al. Spinal cord stimulation for painful diabetic neuropathy. *J. Diabetes Sci. Technol.* **18**, 168–192 (2024).
- Groiss, S. J., Wojtecki, L., Sudmeyer, M. & Schnitzler, A. Deep brain stimulation in Parkinson's disease. *Ther. Adv. Neurol. Disord.* **2**, 20–28 (2009).
- Zangabadi, N. et al. Deep brain stimulation and drug-resistant epilepsy: a review of the literature. *Front. Neurol.* **10**, 601 (2019).
- Frizon, L. A. et al. Deep brain stimulation for pain in the modern era: a systematic review. *Neurosurgery* **86**, 191–202 (2020).
- Lee, U. J. et al. National trends in neuromodulation for urinary incontinence among insured adult women and men, 2004–2013: the urologic diseases in America Project. *Urology* **150**, 86–91 (2021).
- Kang, W. et al. Closed-loop direct control of seizure focus in a rodent model of temporal lobe epilepsy via localized electric fields applied sequentially. *Nat. Commun.* **13**, 7805 (2022).
- Cameron, T. Safety and efficacy of spinal cord stimulation for the treatment of chronic pain: a 20-year literature review. *J. Neurosurg.: Spine* **100**, 254–267 (2004).
- Mickle, A. D. et al. A wireless closed-loop system for optogenetic peripheral neuromodulation. *Nature* **565**, 361–365 (2019).
- Song, H. et al. Neuromodulation of the peripheral nervous system: Bioelectronic technology and prospective developments. *BMEat* **2**, e12048 (2024).
- Sanford, M. T. & Suskind, A. M. Neuromodulation in neurogenic bladder. *Transl. Androl. Urol.* **5**, 117–126 (2015).
- De Ferrari, G. M. et al. Chronic vagus nerve stimulation: a new and promising therapeutic approach for chronic heart failure. *Eur. Heart J.* **32**, 847–855 (2011).
- Mun, J., Lee, J., Park, E. & Park, S.-M. Frequency-dependent depression of the NTS synapse affects the temporal response of the antihypertensive effect of auricular vagus nerve stimulation (aVNS). *J. Neural Eng.* **19**, 046039 (2022).
- de Groat, W. & Tai, C. Impact of bioelectronic medicine on the neural regulation of pelvic visceral function. *Bioelectron. Med.* **2**, 25–36 (2015).
- Park, E. et al. The long-lasting post-stimulation inhibitory effects of bladder activity induced by posterior tibial nerve stimulation in unanesthetized rats. *Sci. Rep.* **10**, 19897 (2020).
- Lee, J. et al. An efficient noninvasive neuromodulation modality for overactive bladder using time interfering current method. *IEEE Trans. Biomed. Eng.* **68**, 214–224 (2021).
- Janknegt, R. A. et al. Long-term effectiveness of sacral nerve stimulation for refractory urge incontinence. *Eur. Urol.* **39**, 101–106 (2001).
- Alqahtani, T. F. et al. Knowledge and perception toward neuromodulation devices among medical students at Umm Al-Qura University. *Cureus* **15**, e45256 (2023).

23. Charvet, L. E., Shaw, M. T., Bikson, M., Woods, A. J. & Knotkova, H. Supervised transcranial direct current stimulation (tDCS) at home: A guide for clinical research and practice. *Brain Stimulation* **13**, 686–693 (2020).
24. Ahmed, Z. Electrophysiological characterization of spino-sciatic and cortico-sciatic associative plasticity: modulation by trans-spinal direct current and effects on recovery after spinal cord injury in mice. *J. Neurosci.* **33**, 4935 (2013).
25. Im, J. J. et al. Effects of 6-month at-home transcranial direct current stimulation on cognition and cerebral glucose metabolism in Alzheimer's disease. *Brain Stimul.* **12**, 1222–1228 (2019).
26. Weil, E. H. et al. Sacral root neuromodulation in the treatment of refractory urinary urge incontinence: a prospective randomized clinical trial. *Eur. Urol.* **37**, 161–171 (2000).
27. Banakhar, M. A., Al-Shaiji, T. & Hassouna, M. Sacral neuromodulation and refractory overactive bladder: an emerging tool for an old problem. *Ther. Adv. Urol.* **4**, 179–185 (2012).
28. Hijaz, A. et al. Complications and troubleshooting of two-stage sacral neuromodulation therapy: a single-institution experience. *Urology* **68**, 533–537 (2006).
29. Hassouna, M. M. et al. Sacral neuromodulation in the treatment of urgency-frequency symptoms: a multicenter study on efficacy and safety. *J. Urol.* **163**, 1849–1854 (2000).
30. Colicchio, G. et al. Vagal nerve stimulation for drug-resistant epilepsies in different age, aetiology and duration. *Child's Nerv. Syst.* **26**, 811–819 (2010).
31. Ghaemi, K. et al. Vagus nerve stimulation: Outcome and predictors of seizure freedom in long-term follow-up. *Seizure* **19**, 264–268 (2010).
32. Fjorback, M. V. et al. Electrical stimulation of sacral dermatomes in multiple sclerosis patients with neurogenic detrusor overactivity. *Neurol. Urodyn.* **26**, 525–530 (2007).
33. Lo, M.-C. & Widge, A. S. Closed-loop neuromodulation systems: next-generation treatments for psychiatric illness. *Int. Rev. Psychiatry* **29**, 191–204 (2017).
34. Versantvoort, E. M. et al. Evoked compound action potential (ECAP)-controlled closed-loop spinal cord stimulation in an experimental model of neuropathic pain in rats. *Bioelectron. Med.* **10**, 2 (2024).
35. Matarazzo, J. V. et al. Combined optogenetic and electrical stimulation of the sciatic nerve for selective control of sensory fibers. *Front. Neurosci.* **17**, 1190662 (2023).
36. Mirza, K. B., Golden, C. T., Nikolic, K. & Toumazou, C. Closed-loop implantable therapeutic neuromodulation systems based on neurochemical monitoring. *Front. Neurosci.* **13**, 808 (2019).
37. Oh, S. et al. Bioelectronic implantable devices for physiological signal recording and closed-loop neuromodulation. *Adv. Funct. Mater.* **34**, 2403562 (2024).
38. Zanos, S. Closed-loop neuromodulation in physiological and translational research. *Cold Spring Harb Perspect Med.* **9**, a034314 (2019).
39. Scarneciu, I. et al. Overactive bladder: A review and update. *Exp. Therapeutic Med.* **22**, 1–8 (2021).
40. Amarenco, G. et al. Urodynamic effect of acute transcutaneous posterior tibial nerve stimulation in overactive bladder. *J. Urol.* **169**, 2210–2215 (2003).
41. McClurg, D. et al. Stimulation of the tibial nerve—a randomised trial for urinary problems associated with Parkinson's—the STARTUP trial. *Age Ageing* **51**, afac114 (2022).
42. McPhail, C. et al. The investigation of percutaneous tibial nerve stimulation (PTNS) as a minimally invasive, non-surgical, non-hormonal treatment for overactive bladder symptoms. *J. Clin. Med.* **12**, 10 (2023).
43. Li, X., Li, X. & Liao, L. Mechanism of action of tibial nerve stimulation in the treatment of lower urinary tract dysfunction. *Neuromodul.: Technol. Neural Interface* **27**, 256–266 (2024).
44. Al-Danakh, A. et al. Posterior tibial nerve stimulation for overactive bladder: mechanism, classification, and management outlines. *Parkinsons Dis.* **2022**, 2700227 (2022).
45. Krivoborodov, G. in *Handbook of Neurology: Theory and Practice* (eds L. Liao & H. Madersbacher) 395–400 (Springer Nature Singapore, 2023).
46. Günter, C., Delbeke, J. & Ortiz-Catalan, M. Safety of long-term electrical peripheral nerve stimulation: review of the state of the art. *J. Neuroeng. Rehabil.* **16**, 13 (2019).
47. Zecca, C. et al. Motor and sensory responses after percutaneous tibial nerve stimulation in multiple sclerosis patients with lower urinary tract symptoms treated in daily practice. *Eur. J. Neurol.* **21**, 506–511 (2014).
48. Ravagli, E. et al. Imaging fascicular organization of rat sciatic nerves with fast neural electrical impedance tomography. *Nat. Commun.* **11**, 6241 (2020).
49. Steffens, H., Dibaj, P. & Schomburg, E. D. In vivo measurement of conduction velocities in afferent and efferent nerve fibre groups in mice. *Physiol. Res* **61**, 203–214 (2012).
50. de Groat, W. C. & Yoshimura, N. Afferent nerve regulation of bladder function in health and disease. *Handb Exp Pharmacol.* 91–138 (2009).
51. Arya, N. G. & Weissbart, S. J. Central control of micturition in women: Brain-bladder pathways in continence and urgency urinary incontinence. *Clin. Anat.* **30**, 373–384 (2017).
52. Won, J. C. & Park, T. S. Recent advances in diagnostic strategies for diabetic peripheral neuropathy. *Endocrinology and Metabolism (Seoul, Korea)* **31** (2016).
53. Moazzam, Z., Duke, A. R. & Yoo, P. B. Inhibition and excitation of bladder function by tibial nerve stimulation using a wirelessly powered implant: an acute study in anesthetized cats. *J. Urol.* **196**, 926–933 (2016).
54. Su, X., Nickles, A. & Nelson, D. Neuromodulation in a rat model of bladder micturition reflex. *Am. J. Physiol. Ren. Physiol.* **302**, F477–F486 (2011).
55. Moazzam, Z. & Yoo, P. Prolonged inhibition of bladder function is evoked by low-amplitude electrical stimulation of the saphenous nerve in urethane-anesthetized rats. *Physiological Rep.* **10**, e15517 (2022).
56. Reichert, W. M. *Indwelling neural implants: strategies for contending with the in vivo environment*. (CRC Press, 2007).
57. Oh, J. et al. Air-Permeable Waterproofing Electrocardiogram Patch to Monitor Full-Day Activities for Multiple Days. *Adv. Healthc. Mater.* **11**, 2102703 (2022).
58. Ju, M.-S., Lin, C.-C. K., Fan, J.-L. & Chen, R.-J. Transverse elasticity and blood perfusion of sciatic nerves under in situ circular compression. *J. Biomech.* **39**, 97–102 (2006).
59. Wang, X. & Hong, W. A visco-poroelastic theory for polymeric gels. *Proc. R. Soc. A: Math., Phys. Eng. Sci.* **468**, 3824–3841 (2012).
60. Lee, J. I. et al. Visco-poroelastic electrochemiluminescence skin with piezo-ionic effect. *Adv. Mater.* **33**, 2100321 (2021).
61. Topp, K. S. & Boyd, B. S. Structure and biomechanics of peripheral nerves: nerve responses to physical stresses and implications for physical therapist practice. *Phys. Ther.* **86**, 92–109 (2006).
62. Fleming, P. et al. Strain on the human sciatic nerve in vivo during movement of the hip and knee. *J. Bone Jt. Surg. Br.* **85-B**, 363–365 (2003).

Acknowledgements

This research was supported by National R&D Program through the National Research Foundation of Korea (NRF) funded by Ministry of Science and ICT (Grant No. NRF-2021M3H4A1A03049084). S.-M.P. acknowledges support from the Pioneer Research Center Program through the National Research Foundation of Korea funded by the Ministry of Science, ICT & Future Planning (2022M3C1A3081294). D.H.K. acknowledges support from the Basic Science Research Program of the

National Research Foundation of Korea (NRF) funded by the Ministry of Science and ICT (RS-2024-00405818). Also, D.H.K. acknowledges support from the Yangyoung Foundation.

Author contributions

Y.-S.L. and J.K. designed the study and implemented the in vivo experiments. Y.-S.L. and J.K. developed implantable devices. J.H.K. and W.H.C. developed implantable electrode. Y.-S.L. and M.H. developed implantable packaging. M.H. and W.K. developed a wireless power transfer system. Y.-S.L. and J.H.K. performed in vivo experiments. M.K. conducted histological analysis. J.H.K. performed the material characterization studies. Y.-S.L. analyzed in vivo experiment data and prepared figures. Y.-S.L. and J.H.K. wrote the manuscript. S.P. contributed to sensor design. U.J. contributed to electrode material fabrication. S.-M.P. and D.H.K. supervised the whole research.

Competing interests

The authors declare no competing interests.

Ethics

Every experiment involving animals, or clinical samples have been carried out following a protocol approved by an ethical commission (POSTECH IACUC).

Additional information

Supplementary information The online version contains supplementary material available at <https://doi.org/10.1038/s41467-025-59436-4>.

Correspondence and requests for materials should be addressed to Do Hwan Kim or Sung-Min Park.

Peer review information *Nature Communications* thanks Hsien-Yu Peng, and the other, anonymous, reviewer(s) for their contribution to the peer review of this work. A peer review file is available.

Reprints and permissions information is available at <http://www.nature.com/reprints>

Publisher's note Springer Nature remains neutral with regard to jurisdictional claims in published maps and institutional affiliations.

Open Access This article is licensed under a Creative Commons Attribution-NonCommercial-NoDerivatives 4.0 International License, which permits any non-commercial use, sharing, distribution and reproduction in any medium or format, as long as you give appropriate credit to the original author(s) and the source, provide a link to the Creative Commons licence, and indicate if you modified the licensed material. You do not have permission under this licence to share adapted material derived from this article or parts of it. The images or other third party material in this article are included in the article's Creative Commons licence, unless indicated otherwise in a credit line to the material. If material is not included in the article's Creative Commons licence and your intended use is not permitted by statutory regulation or exceeds the permitted use, you will need to obtain permission directly from the copyright holder. To view a copy of this licence, visit <http://creativecommons.org/licenses/by-nc-nd/4.0/>.

© The Author(s) 2025